Optimisation of growth parameters to obtain epitaxial Y-doped $BaZrO_3$ proton conducting thin films

A. Magrasó,[a,b,*] B. Ballesteros,[a] R. Rodríguez-Lamas,[a] M. F. Sunding,[c] J. Santiso[a]

a Catalan Institute of Nanoscience and Nanotechnology (ICN2); CSIC and Barcelona Institute of Science and Technology (BIST), Bellaterra-08193, Spain

b Department of Chemistry, Centre for Materials Science and Nanotechnology (SMN), University of Oslo, FERMiO, Gaustadalléen 21, NO-0349 Oslo, Norway

c SINTEF Materials & Chemistry, Forskningsveien 1, NO-0373 Oslo, Norway

Abstract

We hereby report developments on the fabrication and characterization of epitaxial thin films of proton conducting Y-doped $BaZrO_3$ material (BZY) by pulsed laser deposition (PLD) on different single crystal substrates (MgO, $GdScO_3$, $SrTiO_3$, $NdGaO_3$, $LaAlO_3$ and sapphire) using Ni-free and 1% Ni-containing targets. Pure, high crystal quality epitaxial films of BZY are obtained on MgO and on perovskite-type substrates, despite the large lattice mismatch from 5.5 to almost 10 %. The deposition conditions influence the morphology, cell parameters and chemical composition of the film, the oxygen partial pressure during film growth being the most determining. Film characterization was carried out using X-ray diffraction, transmission electron and atomic force microscopies, electron probe microanalysis and angle-resolved X-ray photoelectron spectroscopy. All films show a slight tetragonal distortion that is not simply related to the substrate strain. High temperature XRD reveals that the realtive thermal expansion of film and substrate plays an important role in determining film structure. The proton conductivity of the films depends on deposition conditions and film thickness, and for the optimised conditions the conductivity is slightly higher than the bulk conductivity of the Ni-free target (3 mS/cm at 600 °C, in wet 5% H_2/Ar).

1. Introduction

Acceptor-doped $BaZrO_3$ is one of the state-of-the-art proton conducting oxides for use as electrolyte in proton conducting solid oxide fuel cells.[1] The main advantages are the high bulk conductivity (>10 mS/cm above 400°C for 20%Y in $BaZrO_3$ ceramics) and the high chemical stability towards acidic gases, such as CO_2.[2] $BaZrO_3$ is, however, troubled by resistive grain boundaries that limit the performance of the material.[3-5]

The search for new strategies to engineer thin films and interfaces with nano-effects in oxide materials is a very active field of research, with outstanding examples of increased oxide ion conductivity in doped ZrO_2 or CeO_2.[6,7] The space charge layer effect,[8] generally occurring at the substrate-film interface or at the grain boundary regions, intends to rationalise this experimental enhancement with the variation of the charge carriers' density, or their mobilities, at the interface, which become increasingly dominant with decreasing the thickness/particle size. Other studies rationalise such effect to tensile strain induced from the substrate to the film.[9] The reasoning behind large variations of the conductivity in nano-sized oxides is still under big debate among the scientific community, and therefore demands further investigations dedicated to the fundamental understanding of the phenomena.

Dedicated studies of the effect of strain and related interfacial effects in epitaxially-grown proton conducting thin film oxides are relatively scarce in literature, even for the widely studied Y-doped $BaZrO_3$ (BZY). From the experimental point of view, only a few reports are available, with significant differences among them. Shim et al[10] reported that highly textured 60 nm BZY film epitaxially grown on MgO(100) showed high ionic conductivity (in the order of 1 mS/cm at 200 °C), very close the bulk values reported by Kreuer.[2] Similarly, Pergolesi et al[11] reported that epitaxial ~1 µm BZY thin films on MgO (100) showed very high total conductivity (110 mS/cm at 500 °C), eventually matching the extrapolated bulk protonic conductivity.[2] They report that these conductivities (the highest ever reported so far for BZY) may be understood as a direct measurement of the bulk conductivity of a *de-facto* grain boundary free BZY *via* the fabricated epitaxial thin film. On the other hand, Bae et al[12] reported that polycrystalline BZY films, obtained by PLD on MgO (100) at 700 °C under various oxygen

partial pressures (10-300 mtorr), exhibit a very low conductivity below 0.1 mS/cm at 650°C, close to that reported for 30 nm nanograined BZY thin films.[2]

This discrepancy of more than three orders of magnitude in the total conductivity evidences the influence of film microstructure. This work will focus on the study of the effect of strain and microstructural modifications of $BaZr_{0.9}Y_{0.1}O_3$ thin films, obtained by pulsed laser deposition on different substrates, in the search for possible implications in the protonic conductivity. This report contains an extensive study of the structural and microstructural characterization of the films, both ex-situ (at room temperature) and in-situ (at high temperature) under realistic operation conditions. The study is complemented with the electrical conductivity study of the films and a comparison with recent literature.

2. Experimental

The films were grown using a Compex Pro 201 KrF excimer laser (248 nm) at 1 Hz pulse repetition rate at laser fluence 1-2 J/cm^2 (measured directly at the target spot). We ablated a target of $BaZr_{0.9}Y_{0.1}O_{3-\delta}$ (thereafter referred as BZY) prepared by two different methods: Ni-free and Ni-containing bulk targets. A Ni-free target was prepared by Dr. Ricote at the Colorado Fuel Cell Center (USA) by sintering a disk pellet at 1670 °C of stoichiometric BZY powder in a bed of BZY with $BaCO_3$ to avoid Ba-evaporation, as similarly reported in.[13] The density after sintering was ~85% and the diameter was 25 mm. A second target was prepared by Dr. Manerbino at CoorsTek Inc. (USA) by preparing a pellet using solid state reactive sintering with 1 wt % NiO at 1500 °C, as described in ref.[14] The density after sintering was >98 % and the diameter was 24 mm. In this case the Ni addition was only intended for lowering the sintering temperature and no effect in the protonic conductivity is expected. The deposition was carried out in oxygen partial pressures from 10 to 380 mTorr of O_2, by using either pure O_2, or O_2/Ar mixtures. Substrate temperatures were varied from 600-800 °C, and the heating and cooling rate was 10 °C/min. Target to substrate distance was set to 57 mm. The thickness variation was achieved by varying the number of pulses from 100 up to 15000 pulses. Unless stated otherwise, “standard” growth conditions are the following: 500 pulses, 100 mtorr (pure O_2), 700 °C and Ni-free target.

The substrates examined in this study comprise commercial single crystals of MgO (100), $GdScO_3$ (GSO) (110), $SrTiO_3$ (STO) (100), $NdGaO_3$ (NGO) (110), sapphire $(1\bar{1}02)$ – also called r-cut sapphire- and $LaAlO_3$ (LAO) (012), all purchased from CrysTec GmbH (Germany). The different substrates exhibit a wide range of cell parameters so that the influence of substrate mismatch in the film growth and properties can be explored. **Table 1** shows the relative mismatch between the BZY and the selected substrates.

After deposition, the films were analysed by X-ray diffraction (XRD) using a PANalytical X`PERT PRO MRD diffractometer. Standard 2θ-ω scans from 15 to 120° were performed using a Cu tube with a W/Si parabolic mirror (with Cu $K_{\alpha1}$ and $K_{\alpha2}$ radiations). High resolution 2θ-ω scans and reciprocal space mapping of different asymmetric H0L reflections were performed using a 2-crystal monochromator (2xGe220) for selected samples and peaks. The thickness of the films was examined by X-ray reflectometry (XRR), and the surface

Table 1. Different substrates for BZY, mismatch and strain type, calculated from the in-plane lattice parameters of the substrate (pseudocubic in-plane cell parameters for the

Substrate	In-plane parameter (Å)	Structure type	Mismatch (%)	Strain on BZY
r-cut sapphire	3.500	Corundum	-16.7	Compressive
(012) LAO	3.790	perovskite	-9.8	Compressive
(110) NGO	3.858	perovskite	-8.2	Compressive
(001) STO	3.905	perovskite	-7.0	Compressive
(110) GSO	3.971	perovskite	-5.5	Compressive
(100) MgO	4.210	Rock-salt	+0.2 %	~negligible

distorted perovskites) and taking BZY cell parameter as 4.2017 Å,[16] at room temperature.

topography explored by atomic force microscopy (AFM) using a MFP-3D Asylum instrument in tapping mode.

Sample cross sections for transmission electron microscopy (TEM) were prepared using standard grinding, cutting and ion milling procedures. Samples were afterwards examined using a FEI Tecnai G^2 F20 with a field emission gun (FEG) high resolution and analytical TEM/STEM operated at 200 kV. Low- and high-angle annular dark field images were acquired using inner detector acceptance angle of around 15 and 95 mrad respectively.

The average chemical composition of some of the thin film samples was analysed by wavelength dispersive X-ray spectroscopy (WDS) using a Cameca SX100 apparatus. The surface and sub-surface composition was characterised by parallel angle-resolved X-ray photoelectron spectroscopy (ARXPS) using a Thermo Scientific Thetaprobe spectrometer. Spectra were acquired at 16 angles evenly spread between 22° and 78° emission angle with respect to the surface normal. The spectra were obtained with monochromatic Al Kα radiation and using a combination of low energy electrons and Ar^+ ions for charge compensation. The spectra were energy reference based on the position of the C 1s alkyl peak from adventitious carbon, set to 284.8 eV binding energy (BE). Data treatment was performed using the Thermo Scientific Avantage software (version 5.951). The required number of independent peak fitting components was determined using primary component analysis (PCA) before peak fitting itself was performed. The separation and intensity ratio of the spin orbit pairs was fixed to the values suggested by the software and the positions and peak widths were kept constant for all angles in each sample during the peak fitting.

In-situ high temperature X-ray diffraction (HTXRD) was performed with a PANalytical X`PERT PRO MRD diffractometer with an Anton Paar hot stage (DHS1100) and a graphite dome that allows for analysis under controlled gas atmospheres at high temperatures. X-ray reciprocal space maps were collected for BZY/MgO and BZY/NGO films during cooling down from from 800 °C to RT under a constant flow of N_2 with controlled humidity levels: either dry (bubbling through P_2O_5 powder) or wet (bubbling through a KBr saturated water solution) nitrogen. The maps were measured at selected temperatures after 30 min equilibration time. The first temperature ramp was taken in dry N_2, followed by wet N_2.

Selected films were prepared for electrical measurements in a 2-point 4-wire setup using both in-plane (MgO substrate) and across-plane (conducting Nb-doped STO substrate) configurations. Thin layer Pt electrodes were first deposited by PLD, followed by painting a thicker coating with Pt ink (reference 6926 from Metalor) and afterwards firing the film at 700 °C for 30 min. The conductivity was measured using an impedance spectrometer (Zahner Zennium electrochemical workstation) in a ProboStat^{TM} measurement cell (NorECs, Norway). Impedance spectra were recorded in the 1 MHz to 0.1 Hz frequency range with an oscillation voltage of 50 mV in various atmospheres, including humidified/dried air, N_2/Ar, and 5% H_2/Ar.

3. Results

3.1 Structural and microstructural characterization of BZY films as a function of substrate type.

Figure 1 shows the XRD patterns obtained for the film deposited on various tested substrates at standard conditions (100 mtorr of pure O_2, 700 °C, Ni-free target), which serves to analyse the film composition and preferential growth direction. The most intense reflections correspond to the substrate, while the reflections corresponding to BZY (00L) are marked in the graph. This shows that all the substrates (except sapphire) induce a growth of pure perovskite BZY phase with a high preferential orientation. The BZY structure is oriented on the primitive pseudocubic structure of the substrate, regardless of their relative mismatch (see a zoomed-in graph in **Figure S1a**), showing cube-on-cube growth. In the case of MgO substrate, two different targets were used. This serves to test a possible influence of the target properties to the film. From **Figure S1b**, there is no visible difference between the films from the XRD perspective. However, we should mention that a weak but detectable peak at 2θ~30° appears in both cases (and most films when using the MgO substrate). This may be assigned to a residual (011) reflection of the BZY film. Its origin is most likely induced by defects on the MgO surface rather than to the target or to the growth conditions, since the films grown on the perovskite substrates (GSO, STO, NGO, LAO) do not show this additional peak. The orientation of the film deposited on r-cut sapphire was determined by

General Area Detector Diffraction System (GADDS) and concluded to be polycrystalline (see **Figure S2** for further details). The high resolution XRD scans of the highly textured films (**Fig. 1b**) show distinct thickness fringes for the BZY (002) reflection, demonstrating the high crystalline quality of the deposited films. The fringes are not visible in the case of the MgO substrate either due to the strong overlap of the substrate and film reflection, as expected from their excellent lattice match, or to the fact that the film has some defects that break the crystal coherence in the vertical direction. It is remarkable that all BZY films grow with such good quality and orientation, despite the large lattice mismatch with the perovskite single crystal

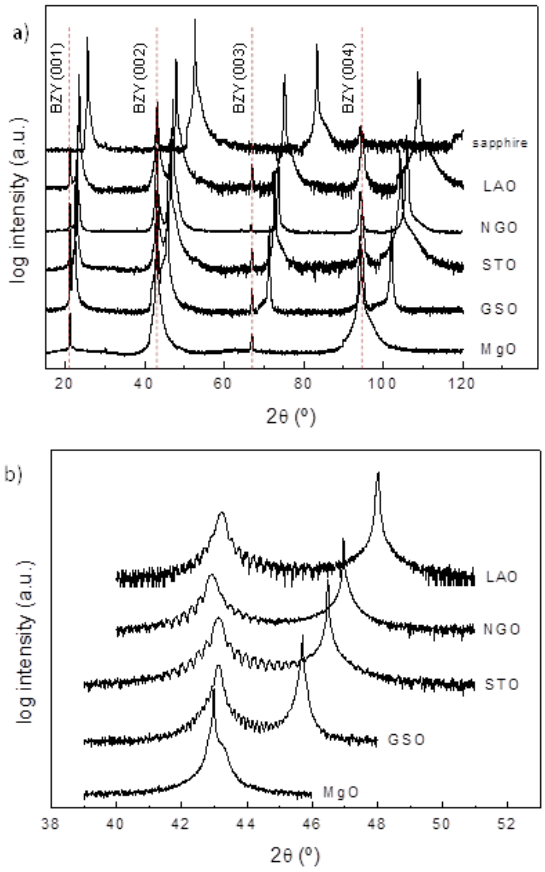

Fig. 1. a) Standard 2theta-omega XRD scans for the various tested substrates and b) high-resolution scans of the epitaxially grown films around the BZY (002) reflection

substrates, as high as ~-10 % on LAO (see **Table 1**). The effect of deposition temperature was studied at 600, 700 and 800 °C on MgO and LAO, with no apparent effect in the XRD patterns nor the cell parameters (not shown).

XRR scans are performed to determine the thickness of the films as a function of substrate type (**Figure S3**). In correlation with the comments above, reflectivity measurements show very well defined fringes for the epitaxial films, which suggest that the films are very homogenous in thickness with low surface roughness. On sapphire, the XRR scan does not show oscillations, which may be connected to the higher roughness and the polycrystalline nature of this film. Additional XRR scans were performed as a function of number of pulses and the variation of the laser fluence (see **Figure S4** as representative examples), showing that the film thickness shows a linear variation with both parameters.

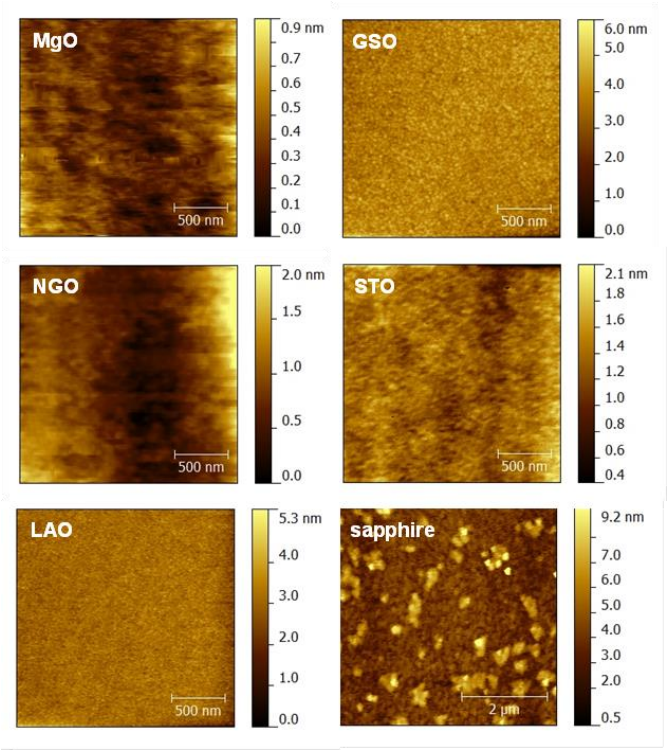

Fig. 2. AFM micrographs of the top surface of the BZY films grown over the different tested substrates

Figure 2 shows AFM micrographs of the as-grown BZY film surface as a function of substrate type. BZY grown on sapphire shows a surface with relatively high roughness (Rms=2.3 nm) as inferred from the XRR results. This likely shows the disturbance of the

preferential orientation shown by the XRD measurements (**Fig. S2**). The films grown on perovskite substrates show a very smooth and flat surface (Rms=0.1-0.3 nm), in agreement with the XRR measurements reported above (c.f. **Table S1**). It is interesting to report that the roughness seems to increase with the number of pulses, as typically observed in vapour grown polycrystalline films, while unaffected by the fluence, from 1 to 2 J-cm^2 (**Fig. S4**).

High resolution cross-section TEM micrographs of selected BZY/substrate interfaces are shown in **Figure 3** (additional micrographs are provided as supplementary material in a separate file). The specimens were oriented to be in [100]-zone axis. Overall, the HRTEM analysis confirms that the films are highly textured in all the cases, with well aligned atomic columns following the substrate orientation (confirmed by electron diffraction) as corresponds to the cube-on-cube epitaxy. The BZY/MgO interface looks relatively sharp and defect free compared to the BZY/perovskite interfaces that are under strong compressive strain (~5-10 %). The latter show a high concentration of defects, mostly consisting of misfit dislocations that are periodically distributed along the interface. These are particularly visible on the BZY/NGO cross-section (dark spot regions at the interface), with an average distance of about 13 unit cells of the primitive NGO structure. This value is very close to the expected distance of about 12 unit cells of typical misfit dislocation with [100] Burgers vector, which would correspond to the full strain release for the -8.2% mismatch of BZY and NGO equilibrium structures. However, the BZY/STO interface shows a more complex contrast effect at the interface forming alternating bright and dark contrast vertical stripes in a region about 5-7 nm thick at the interface, very likely due to a dissociation of dislocations into partial components. Low- and high-angle annular dark field (LAADF and HAADF) imaging in STEM mode provides further information of the defects (in the supplementary information **Figure S5**). Defects are more evident in LAADF images in which contrast arises by strain effects, whereas HAADF images provide information on composition as the intensity is proportional approximately to the square of the atomic number. The layers are, in general, quite homogeneous, while small contrast differences in the

vertical direction exist, which could indicate the presence of linear defects along the layer

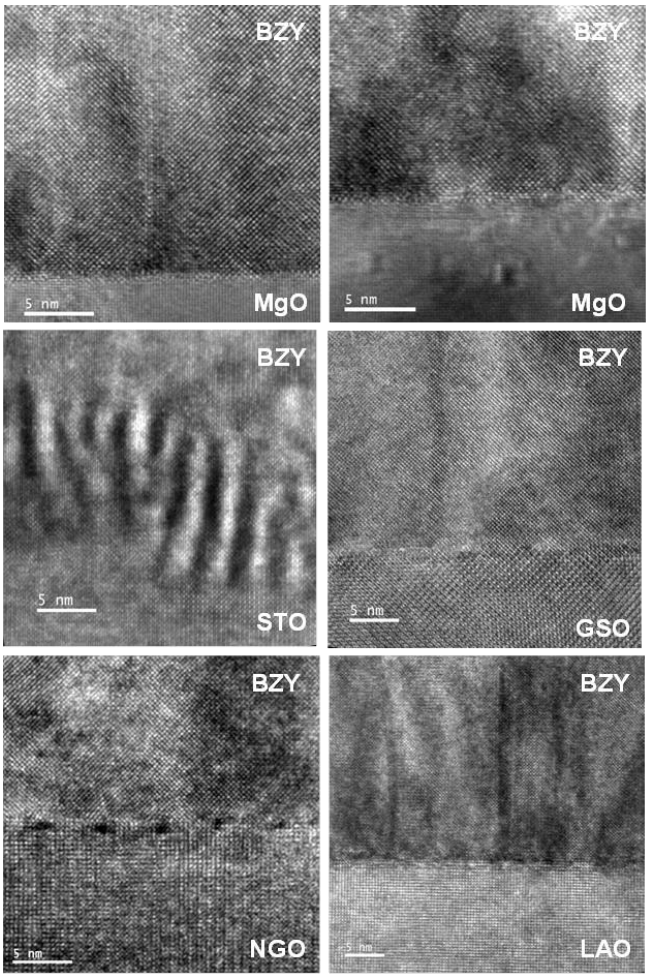

Figure 3. HRTEM micrographs of the BZY/substrate interface as a function of substrate type. The BZY/MgO interfaces correspond to the same specimen in two different areas.

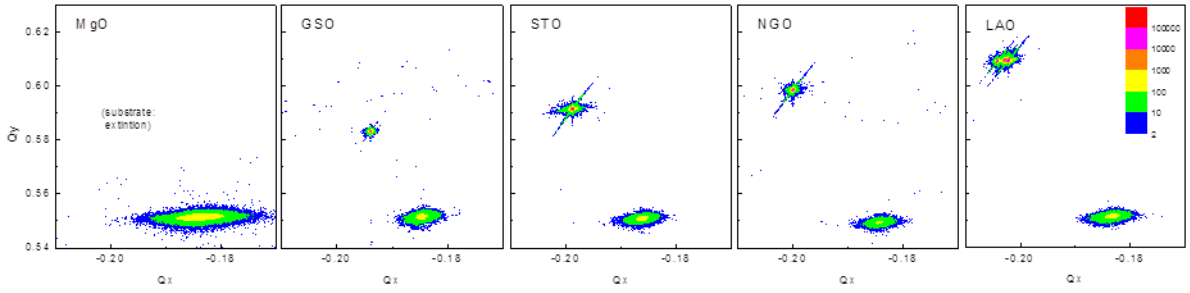

Figure 4. Reciprocal space mapping of the BZY$(\bar{1}03)$ reflection for various substrates.

Focusing now on the BZY grown on MgO, the film shows some defected regions perpendicular to the substrate surface, likely consisting of extended planar defects. These extended vertical
defects (could be -low angle- grain boundaries) may affect the in-plane conducting properties of BZY films grown on MgO, since the planar currents have to cross a relatively high density of these defects. It is worth to mention that MgO is a relatively plasticmaterial and single crystals have a tendency to exhibit different domains and other defects. This was evident during HRTEM observations that the substrate was not perfect (cf. Fig. 3), and one may speculate whether the source of the line defects observed in the films propagate from defects already present on the substrate, or generated during film growth.

The XRD comparison of the films deposited on different substrates reveal additional features. **Figure 4** shows reciprocal space maps (RSM) of the $\bar{1}03$ BZY reflection that was used for the in-plane cell parameter determination. The most intense and narrower peaks correspond to the $\bar{1}03$ GSO, $\bar{1}03$ STO, $\bar{1}03$ NGO and $\bar{1}03$ LAO substrate reflections (H0L reflections are expressed in terms of the pseudocubic primitive cell), while for MgO this reflection is forbidden. For MgO, additional RSMs were measured for the $\bar{2}04$ reflection (for a representative example, see **Fig. S6**), where peaks from both BZY and MgO appear together. The broader and less intense peaks (c.f. Fig. 4) correspond to the film $\bar{1}03$ BZY reflection. The horizontal and vertical coordinates in the reciprocal space are inversely proportional to the corresponding in-plane and out-of-plane cell parameters in the real structure. The measured cell parameters are included in Table 2. Therefore, it is clearly visible that the cell parameter difference between the BZY film and each substrate increases according to the predicted mismatch (c.f. Table 1) in the order LAO>NGO>STO>GSO. The magnitude of the measured film cell

Table 2. Variation of the in-plane and out-of-plane lattice parameters

Substrate	Thickness (nm)	In-plane (Å)	Out-of--plane (Å)
MgO	55	4.166	4.200
GSO	67	4.168	4.192
STO	38	4.161	4.194
NGO	37	4.195	4.206
LAO	44	4.189	4.193

parameters are very close to each other indicates that BZY is almost fully relaxed in all the cases (including MgO, see **Table 2**). Only subtle differences are detected among the samples and with no apparent correlation with the substrate mismatch. The multi-peak feature observed for LAO$(\overline{1}03)$ reflects the twinning of the crystals with slight misorientations which is characteristic of this material with rhombohedral structure.The peak position of LAO substrate is taken as the centroid of all these peaks instead of the peak with the highest intensity. Among the differences in the comparison of the RSMs, it is evident that the BZY/MgO film exhibits an apparent broadening of the peak shape along the Qx direction compared to those films grown on perovskite substrates. This may indicate inhomogeneities in the direction parallel to the substrate surface. We may attribute this fact to the presence of extended vertical defects, as previously observed from TEM observations. It is interesting to notice that for all samples the out-of-plane cell parameter is slightly larger than in-plane parameter evidencing a certain degree of tetragonal distortion.

3.2 Structural and microstructural characterization of BZY films as a function thickness and oxygen partial pressure.

The calculated in-plane and out-of-plane lattice parameters for BZY films grown over MgO (100) and STO (100) as a function of thickness are shown in **Figure 5**. The films grown over MgO show a complex variation with thickness, and this is dependent on the target used. The in-plane parameter (average is 4.17±0.01 Å) is always smaller to the out-of-plane parameter (average is 4.20±0.01 Å), evidencing a certain degree of tetragonal distortion, as previously pointed out. This is somewhat unexpected in terms of substrate mismatch biaxial strain since the lattice match between MgO and BZY is excellent, they both exhibit a cubic structure, and they are reported to grow cube-on-cube.[11] It is worth to mention that this tetragonal distortion in BZY is relatively similar for the thin films grown on the perovskite substrates, even if the lattice mismatch is larger. Interestingly, BZY films grown from the 1%Ni-containing target show larger in-plane parameter with no tetragonal distortion (except for the thinnest film). The tetragonal distortion is essentially constant for films thicker than 100 nm. For thinner films, the out-of-plane lattice parameter seems to increase slightly from 4.195 to 4.21 Å. This is true for values extracted from both RSM and standard 2θ-ω measurements (c.f. Fig. 1) and therefore, this indicates that the differences are not related to an experimental error of the measurement. One may speculate here that the thermal mismatch induced by MgO (TEC ~ $13.9 \cdot 10^{-6}$ K^{-1})[15] to BZY (TEC ~ $8 \cdot 10^{-6}$ K^{-1})[16] upon cooling after film growth could be the cause for the increased tetragonality of the thinner films.

In BZY/STO films, in Figure 5(b), the thickness decrease induces a reduction of the in-plane cell parameter along with an increase in the out-of-plane cell parameters. This is consistent with the presence of a small compressive strain in the in-plane direction, as expected from the -7% mistmatch, even for films with large thickness of about 300nm. Therefore, the tetragonal distortion increases progressively with decreasing thickness, for films below 10 nm. We may point out that the thickest film (350 nm) is grown on Nb-doped STO (100) instead of STO(100), but given the small dopant content and the large difference between BZY and STO, we believe that the trend is still relevant for

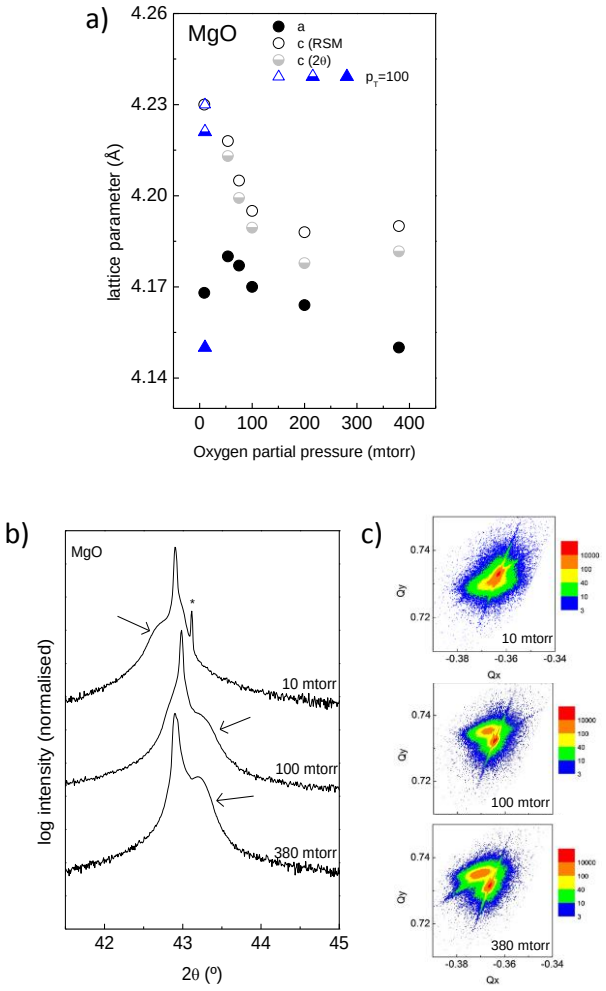

Figure 5. In-plane *a* and out-of-plane *c* lattice parameters of BZY deposited on a) MgO(100) and b) STO(100) substrates calculated from RSM and standard theta-2theta measurements.

overall comparison purposes. Since TEC of BZY and STO (TEC ~ $9 \cdot 10^{-6}$ K^{-1}) are quite similar the increase in the tetragonal distortion for the thinner film could not be related to the thermal mismatch, and therefore it should correspond to a residual compressive strain.

In order to analyse the possible influence of a difference of oxygen stoichiometry in the film characteristics, we explore the variation of lattice parameters as a function of oxygen partial pressure (**Figure 6a**). There is a clear tendency of both the in-plane and

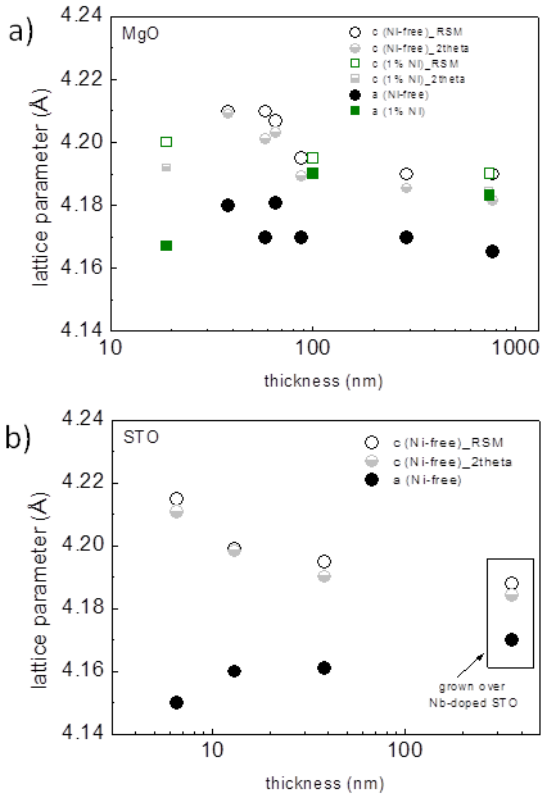

Figure 6. a) In-plane and out-of-plane lattice parameters of BZY/MgO as a function of pO_2. b) Selected high resolution 2theta-omega scans of 002 reflection as a function of pO_2 and c) their corresponding RSM of the $(\bar{2}04)$ reflection. * corresponds to an unknown peak.

out-of-plane parameters (films grown at pO_2> 40 mtorr) to decrease with increasing oxygen partial pressure, the out-of-plane cell parameter being the most sensitive to these changes. This corresponds to an overall cell volume reduction, which possibly indicates changes in the stoichiometry of the as-grown films. Looking at the values calculated from the films grown at pO_2=10 mtorr (total pressure of 100 mtorr, compensated with Ar), they approach those grown at a total pressure of 10 mtorr in pure O_2. Therefore, the lattice constants seem to be more affected by the oxygen content in the chamber during growth rather than by the total pressure. The relatively strong variation of the lattice parameters is consistent when measured from the film

peak position of the high resolution 2θ-ω scans (**Fig. 6b**) and RSM (**Fig. 6c**) as a function of pO_2.

Along with the structural changes, the BZY/MgO films deposited in different pO_2 conditions and different target materials show also changes in the surface morphology, as determined by AFM.

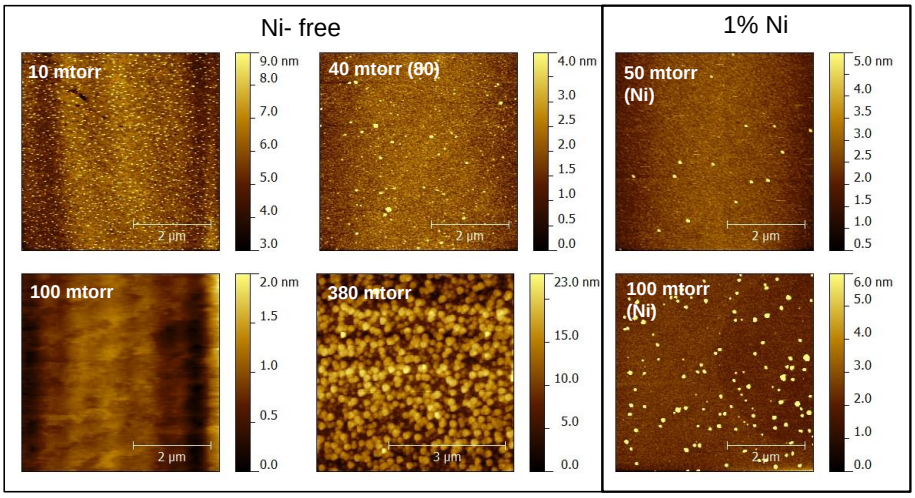

Figure 7. Selected AFM micrographs for the BZY/MgO films deposited in different starting target materials and pO_2 atmospheres (total pressure, when different to oxygen partial pressure, is shown in parenthesis).

The micrographs (**Figure 7**) and the roughness (Table S1) as a function of pO_2 for the Ni-free target show that the film with the smoothest film is grown at ~100 mtorr (Rms=0.3 nm). Growth under lower pO_2 seemingly leads to an overgrowth of small particles (Rms~1nm for pO_2=10 mtorr), although XRD patterns do not show evidence of formation of other phases or orientations, in comparison to those grown at 100 mtorr. Films grown under higher pO_2 (380 mtorr) lead to formation of well-defined, round grains of about 100-200 nm. This is probably undesirable for reaching high conductivities in the films due to the high grain boundary resistance of BZY, widely reported in literature.[3-5] On the other hand, the films grown with the 1% Ni-containing target, show the opposite behavior. The apparent segregation of phases (likely Ni-containing nanoparticles in this case) is reduced by growing the films at lower pO_2.

The composition of the films, as well as the target materials was determined by EPMA (see **Table S2** in the supplementary information). The analysis of the Ni-free target renders $Ba_{0.96\pm0.02}Zr_{0.96\pm0.03}Y_{0.08\pm0.03}O_{3-\delta}$, while the 1% Ni target material renders $Ba_{0.98\pm0.02}Zr_{0.91\pm0.013}Y_{0.099\pm0.016}Ni_{0.009\pm0.004}O_{3-\delta}$. This measurement shows that the Ni-free target is somewhat deficient in barium, while the 1% Ni target is essentially stoichiometric BZY, within error bars.

For the thin film compositions, the oxygen partial pressure during PLD deposition has the strongest impact in the chemical composition (see **Figure 8**), while the laser fluence or the thickness does not seem to affect the stoichiometry significantly (supplementary Table S2). The films grown below 50 mtorr are close to those anticipated from the composition of the initial target materials. However, the films grown at higher pO_2 do show a clear deviation from stoichiometry, especially regarding barium deficiency. This observation is consistent for films grown using both the Ni-free and 1% Ni targets.

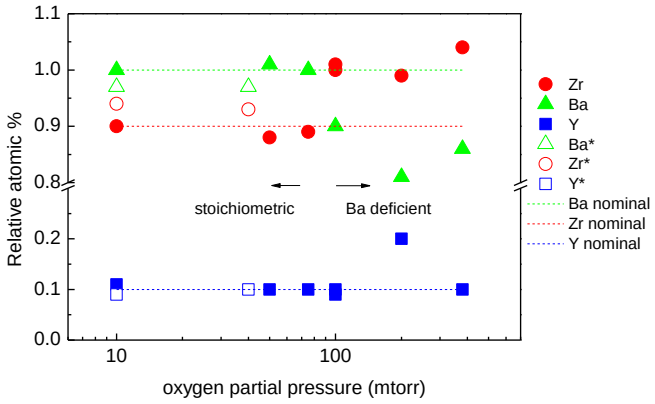

Figure 8. Relative atomic composition of the BZY thin films (Ni-free target) as a function of oxygen partial pressure. Either pure O_2 (filled symbols) or mixtures of O_2/Ar (empty symbols, marked as *) were used.

The chemical composition of the BZY samples grown at pO_2 of 10 mtorr (with compensation with Ar to 100 mtorr) and 100 mtorr was characterised by ARXPS. In both samples Ba, Zr and Y core level spectra were fit to consist of two sets of spin-orbit

split doublets at low and high binding energies, associated to the presence of distinct chemical states (**Table 3, Figure S7**). The lower BE chemical states are consistent with the positions reported for BZY perovskite, while the higher BE peaks fit with e.g. $BaCO_3$, ZrO_2 and Y_2O_3, respectively.[17] In both samples, the variation of the apparent concentrations with the angle of emission show that the high BE chemical states of Ba and Zr are associated with the presence of a surface layer of a few nanometres thickness while all other peaks are located deeper. The precise localisation of the high BE yttrium component is, however, uncertain and can either be attributed to an intermediate layer or to the bulk material, or both. Assuming two distinct yttrium chemical states in BZY this can be attributed to either Y_2O_3 precipitates, yttrium associated with oxygen vacancies or to yttrium localised at Ba sites. Since the presence of precipitates in the film was not observed with TEM it can be dismissed as source for the high BE signal, but the other possibilities remain open without further analyses. The obtained bulk stoichiometries compare well with the EPMA results taking into account the uncertainty in the yttrium signal (**Table 4**). Especially, a higher Ba/Zr ratio is measured in the sample grown at 10 mtorr compared to the one grown at 100 mtorr.

Table 3. Ba, Zr and Y peak positions obtained by ARXPS, in eV BE ±0.3.

pO_2 (mtorr)	**Ba $4d_{5/2}$**		**Zr $3d_{5/2}$**		**Y $3d_{5/2}$**	
	low BE	high BE	low BE	high BE	low BE	high BE
10	88.2	89.7	180.7	181.9	155.4	157.1
100	88.4	89.6	180.6	181.7	155.5	157.2

Table 4. Stoichiometries obtained by ARXPS. The bulk cation ratios are calculated both using only the low BE component of yttrium and using the total determined yttrium content. The relative cation ratio is given in atomic % and normalized to 2 (corresponding to 1Ba, 0.9Zr and 0.1Y), uncertainty ±15%.

pO_2 (mtorr)	**Surface**	**Bulk, only low BE Y**	**Bulk, total Y**

	Ba	Zr	Ba	Zr	Y	Ba	Zr	Y
10	1.4	0.6	1.04	0.85	0.12	1.00	0.82	0.18
100	1.0	1.0	0.97	0.99	0.04	0.92	0.94	0.14

The former sample shows also a clear Ba excess in the surface layer. This implicitly indicates that the source for the Ba deviation is the evaporation of this element at high pO_2.

3.3 High temperature XRD measurements in controlled atmospheres.

In order to obtain structural data at typical operating conditions for high temperature SOFCs or electrolyzers, *in-situ* high temperature X-ray diffraction was performed in a controlled atmosphere. In order to monitor the variations of both the substrate and the film peaks simultaneously, we selected RSM of $\bar{2}04$ reflections for BZY/MgO, while for BZY/NGO we used the $\bar{1}03$ reflections. The calculated lattice parameters for BZY/MgO in dry N_2 are shown in **Fig. 9a**. The variation of both the in-plane and out-of-plane parameters is relatively linear as a function of temperature, although they show an unexpected behaviour. The two trends cross at ~300 ºC, which means that at higher temperatures the film shows a larger in-plane than out-of-plane cell parameters, which progressively reverses at lower temperatures. The curves are essentially equal for the films grown using the Ni-free (c.f. Fig. 9a) or 1% Ni (**Figure S8a**) targets. This behaviour is explained by the difference in the thermal expansion of the film and substrate. At high temperatures (similar to the temperature during film growth in the PLD, i.e. 700 ºC) the BZY film grows partially relaxed and shows an in-plane cell parameter smaller than the MgO substrate, close to the expected equilibrium value at this temperature. However, still a small residual tensile strain produces in-plane stretching and therefore an out-of-plane compression (tetragonal distortion with $c<a$). Upon cooling down from this temperature the film in-plane cell parameter follows the MgO substrate thermal expansion coefficient (also plotted in Fig. 8a). This is because no additional misfit

dislocations are formed after film growth (they are very costly in terms of energy) and the film remains monolithically locked to that of the substrate upon cooling. Due to the relatively large thermal expansion coefficient of the substrate upon reducing the temperature the film in-plane cell parameter becomes progressively smaller than the equilibrium value, while the original residual tensile strain is compensated by the increasing thermal biaxial compressive stress induced at

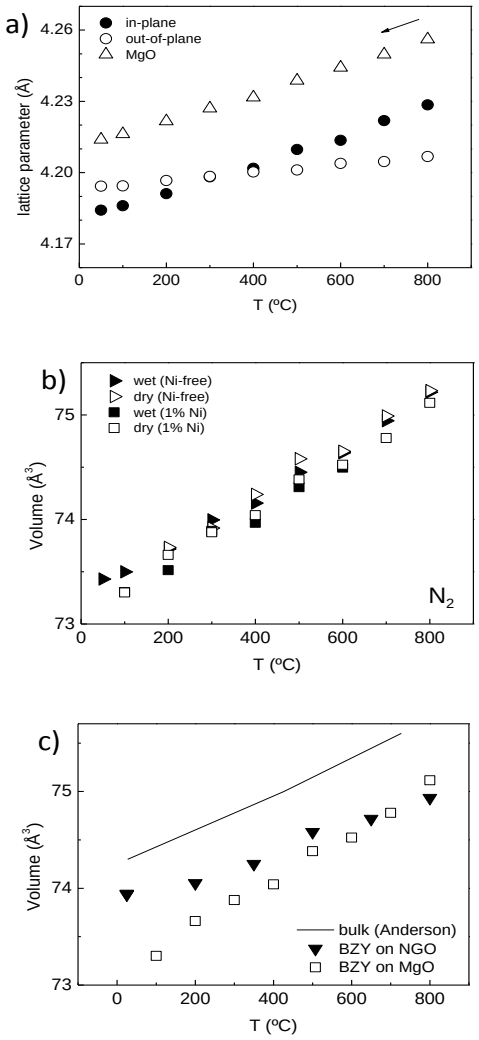

Figure 9. *In-situ* HT-XRD experiments of samples deposited under standard conditions. a) Variation of the in-plane and out-of-plane lattice parameter of BZY deposited on MgO along with that of the substrate in dry N_2. b) Variation of the cell volume with temperature depending on the BZY target (Ni-free and 1% Ni containing targets) and humidity level (wet or dry N_2) on MgO. c) Variation of the cell volume as a function of substrate type, in comparison to bulk BZY10 from Anderson et al.[16]

the film-substrate interface. At a certain temperature (at 300ºC in these experiments) the strain is suppressed and the film becomes cubic (c=a). Further cooling increases the thermal compressive component and the film reacts elastically by increasing the out-of-plane cell parameter, becoming c>a down to room temperature. In the BZY films deposited on NGO (perovskite structure) the behavior of the lattice constants as a function of temperature is closer to that expected: the in-plane and out-of-plane lattice parameters roughly follow a parallel trend. In this case it is also expected that the BZY film in-plane parameter follows the structure changes of the NGO substrate (TEC ~ $9 \cdot 10^{-6}$ K^{-1}). But the very similar thermal expansion coefficients of both film and substrate perovskite structures makes the film not to deviate very much from its natural thermal expansion behaviour (see **Figure S8b**). In the case treated here, it is also interesting to check whether the BZY film shows chemical expansion at intermediate temperatures and wet conditions, as expected for the hydration of the oxygen vacancies to form protons.[16] **Figure 8b** shows the various curves taken upon cooling in wet or dry conditions, for the films prepared with the Ni-free and 1% Ni targets on MgO substrates. By comparing the wet and dry curves for each target type, it is concluded that none of the films show significant expansion of the average cell volume, which may indicate that hydration (if any) is below the sensitivity limit of the cell parameter determination by using XRD reciprocal space mapping. An interesting comparison to be reported here is that the overall cell volume expansion with temperature depends on the substrate type, compared in **Figure 9c**. The linear thermal expansion coefficient (TEC) can be calculated and is summarized in **Table 5**. As mentioned earlier, the TEC of in-plane lattice parameter of BZY thin films follows that of the substrate, while the out-of-plane expansion coefficient is a combination of the natural thermal expansion of the BZY material and the elastic response to the in-plane biaxial stress. Therefore, it is not surprising that the overall cell volume expansion with temperature depends on the substrate and it shows different values than the one reported for bulk material.[16] Obviously, those differences are much larger for the film deposited on MgO substrate than for NGO, as it is for their relative thermal expansion coefficients

At this point we may speculate whether the vertical defects in the BZY film grown on MgO observed from TEM (c.f. Fig. 3) and RSM (c.f. Fig. 4) are generated during the cooling down step after PLD growth due to thermal stress induced by the large difference in thermal expansion coefficients of substrate and film.

Table 5. Summary of the TECs (in K^{-1}) of the BZY films and substrates obtained from the HTXRD analysis.

Film material	Subst	TEC In-plane	TEC Out-of-plane	TEC Overall	Ref.
BZY	MgO	$14 \cdot 10^{-6}$	$4 \cdot 10^{-6}$		This work
	MgO			$13.4\ 10^{-6}$	This work
	MgO			$13.9\ 10^{-6}$	Touloukian et al[15]
BZY	NGO	$7.4 \cdot 10^{-6}$	$5.2 \cdot 10^{-6}$		This work
	NGO	$7.7 \cdot 10^{-6}$	$8.1 \cdot 10^{-6}$		This work
	NGO			$9 \cdot 10^{-6}$	Crystec GmbH
BZY10	-			$7.4\text{-}8.8 \cdot 10^{-6}$	Andersson et al[16]

3.4 Electrical conductivity measurements in controlled atmospheres.

The electrical conductivity (σ) of the films, measured both in-plane (for MgO) and cross-plane (for Nb-STO) configuration, is calculated using the equation:

$$\sigma = \frac{d}{A} \cdot \frac{1}{R} \qquad (1)$$

where *d* is the distance between electrodes, *R* is the film resistance measured by impedance spectroscopy (without the electrode contribution) and *A* is the area of the

cross-section of the conducting path, assuming that the current is flowing homogenously across the whole section of the film (for deposited electrodes on the top surface this is true when the film thickness is sufficiently small compared to the electrode distance).The geometrical factor for the two configurations differs largely: $A/d_{\text{in-plane}}$~$5\cdot10^{-5}$ cm (100 nm thick film) and : $A/d_{\text{cross-plane}}$~$1\cdot10^{4}$ cm (350 nm thick Nb-STO film) for the in-plane and cross-plane geometries, respectively.

Several BZY films deposited on MgO (100) were measured using the in-plane configuration in the temperature range of 700 to 500 ºC. The variation of the conductivity of the optimised BZY/MgO thin film as a function of temperature in different atmospheres is shown in **Figure 10** as a representative example (additional examples are included as supplementary material, **Fig. S9**). It shows that the conductivity in wet Ar is higher than in dry Ar, which is an indication of dominant protonic conductivity according to the hydration reaction:

$$O_O^x + v_O^{\bullet\bullet} + H_2O(g) \leftrightarrow 2OH_O^{\bullet} \qquad (2)$$

The conductivity also decreases with decreasing pO_2 in the order $\sigma_{air} > \sigma_{Ar} > \sigma_{5\%H2}$, and the difference decreases with decreasing temperature. This is an indication that some electron hole conductivity exists (as a minority defect) in BZY films, in accordance with the reported bulk properties of BZY.[13,18] Assuming that oxygen non-stoichiometry (and therefore the oxygen vacancy concentration $[v_O^{\bullet\bullet}]$) is essentially fixed by the concentration of acceptor dopant ($[Y_{Zr}^{/}]$), the variation of the conductivity with oxygen partial pressure, reflects a variation in the concentration of electron holes at high pO_2, in accordance with the following defect chemical equilibrium reaction:

$$O_O^x + 2h^{\bullet} \leftrightarrow v_O^{\bullet\bullet} + ½O_2(g) \qquad (3)$$

The activation energy of the conductivity increases with decreasing water content in Ar (0.65 and 0.80 eV in wet and dry Ar, respectively), which is in accordance with the hydration effect. The activation energy of the conductivity in wet air is a little higher

than in wet Ar, 0.74 eV, which probably reflects the conductivity of both electron holes (minority defects) and protons (majority defects, concentration-wise). In wet reducing conditions, the activation energy is 0.45 eV, likely reflecting the activation energy for

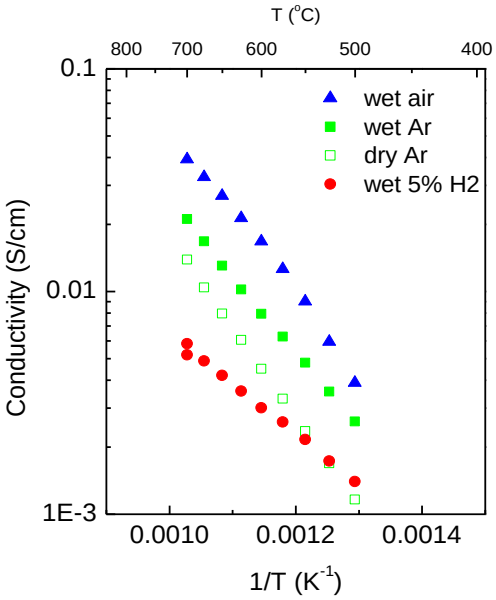

Figure 10. Overall electrical conductivity of the optimised BZY film deposited on MgO (100) measured in various atmospheres. The film is 35 nm thick, and was grown at 700 ºC under 50 mtorr (O_2).

migration of protons, in good agreement with the reference value for bulk BZY (0.46-0.47 eV)[19] and other epitaxial BZY thin film deposited on MgO (0.44-0.46 eV)[10]. Therefore, these conditions will be used to compare the conductivity for the different samples.

The conductivity characteristics of several of the BZY thin films are shown in the supplementary material, and a selection of those are compared in **Figure 11** and **12**. First, the conductivity of the BZY films grown on MgO varies largely depending on the preparation conditions and film thickness. The oxygen partial

pressure used during deposition is a key growth parameter for optimisation of the proton conductivity.

From Figure 11 it is clear that the conductivity first increases and then decreases with the oxygen partial pressure during growth, being optimal (opt) for pO_2= 50 mtorr. This occurs for both the Ni-free and 1% Ni–containing targets. This behaviour could be rationalised based on a trade-off effect between the chemical composition and the

surface characteristics of the films. At low pO_2 (10 mtorr), the films are more stoichiometric but exhibit a rougher surface, which could be an indication of the appearance of (resistive) extended defects within the film. At high pO_2 (380 mtorr), the films are off-stoichiometric (due to Ba losses during PLD growth) and exhibit a nanograined structure, both of these attributes usually correlated with conductivity constriction paths. A loss of barium during the deposition process will, most likely, result in yttrium being incorporated on Ba sites,[20] causing a donor effect and reducing the conductivity.[21] At intermediate pO_2 (50 mtorr), the films are flat and featureless (no grains or nanodomains are visible) while the cation composition is closer to the stoichiometric compound than the films grown at higher pO_2. These conditions lead to the films with the highest conductivities in this work (3.0 and 1.6 mS/cm at 600 ºC in wet reducing conditions, for the Ni-free and 1% Ni target, respectively). The conductivity of the Ni-containing films is lower (by a factor of two) than the Ni-free films, even if the initial target composition is less Ba deficient for the 1%Ni target. Although other factors may affect the conductivity in BZY thin films, it is reported that NiO sintering aid suppresses hydration kinetics of BZY,[22] so the result is within expectations. Furthermore, the conductivity of BZY/MgO decreases with increasing film thickness, along with an increase of the activation energy. The drop in conductivity is very large, of more than two orders of magnitude when the thickness increases from 58 nm to 1.4 µm (Ni-free target, 100 mtorr during deposition). This indicates an increase of the presence of blocking defects in the thicker layer, which could be assigned to resistive grain boundaries (note that even low angle grain boundaries are reported to be resistive[23]) or to other extended defects. This could be in correlation of the vertical defects observed earlier by TEM and RSM. Additionally, the conductivity across the film, measured for one sample of 350 nm-thick BZY deposited on Nb-doped STO(100), is lower than that deposited on MgO (100). This could be assigned either to the relatively thick film used in this configuration or to a resistive interface in accordance with the defective layer between BZY and STO detected in the TEM observations. This point was not pursued further in this work.

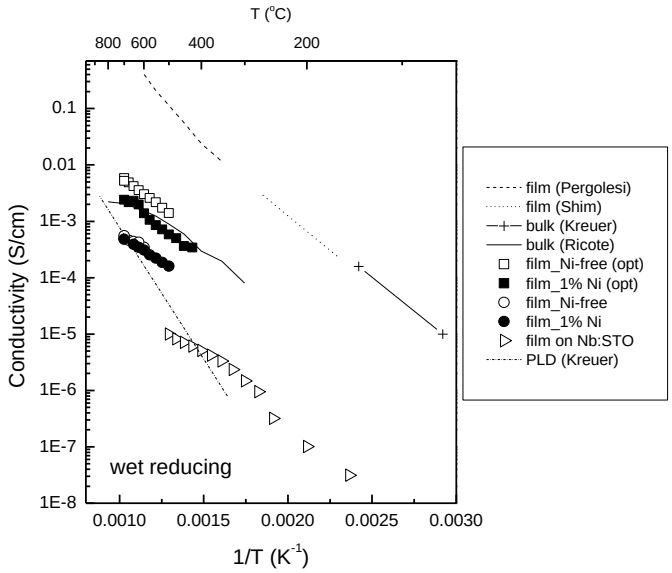

Figure 11. Variation of the conductivity (left axis, symbols) in wet 5%H_2/Ar and the barium deficiency (right axis, lines) of BZY thin films grown on MgO (100) with the oxygen partial pressure during PLD growth. The Ni-free target was used, except the green dots labelled as 600 ºC (Ni). The barium deficiency is calculated as 1-Ba content as measured by EPMA.

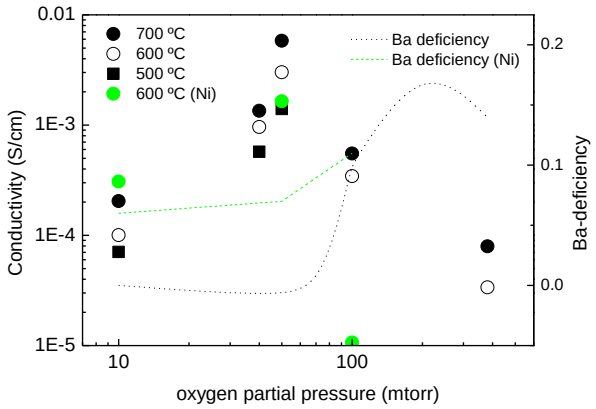

Figure 12. Overall electrical conductivity in wet 5% H_2/Ar (reflecting mainly proton conductivity) of BZY thin films compared to literature (Pergolesi et al.[11], Shim et al.[10], Kreuer[2] and Ricote et al.[13] Films are grown at 100 mTorr, unless labelled as (opt), which refers to the optimised film in terms of the highest conductivity.

4. Discussion

This work clearly shows that BZY grows epitaxially on a number of substrates, even when the lattice mismatch is almost 10%. The BZY films grow cube-on-cube in the (100) direction on MgO (100) and the perovskite substrates (GSO (110), STO (100), NGO (110), LAO (100)), independently of the growth conditions tested in this work. However, the film characteristics are dependent on such conditions. While the laser fluence (1-2 J/cm^2) and substrate temperature (600-800 ºC) do not seem to influence much, the oxygen partial pressure during PLD growth does have an important impact in the lattice parameters of the BZY film, which also influences strongly on the chemical composition and, in turn, on the electrical conductivity.

The BZY films are essentially relaxed (except for the thinnest ones, as expected), but retain some residual strain induced by the substrate and show features that are not corresponding to bulk BZY. The variation of the cell volume of the films with temperature is greatly dependent on the substrate type (c.f. Fig. 9c) and does not correspond to the volume variation of bulk. Additionally, it is remarkable that the residual strain under operation conditions is different than that at room temperature for MgO (100), where standard measurements are taken. This is an important point to highlight from these accurate cell structure measurements, which points out at differences between bulk specimens and epitaxial films, even when they are considered to be “fully relaxed”.

Several researchers have reported conductivities of Y-doped $BaZrO_3$ thin films with large variations of conductivity values (orders of magnitude). This fact is also typically encountered in bulk BZY (see for instance[1,5] and references therein), and there are many factors affecting its proton conductivity.

When comparing the electrical properties of the films in this work with available literature (see some examples in Figure 12), it is clear that the film conductivities under reducing conditions (reflecting essentially protonic conductivity) are, for the optimised BZY/MgO films, slightly higher than the bulk protonic conductivities and activation energies reported by the researchers who fabricated the PLD targets used in this work,[13,14] which is in turn similar to other researchers in the field.[18,24] This is an

indication that the measured conductivities indeed reflect the bulk properties of BZY, without a large enhancement of the conductivity. The conductivity of a nanograined (30 nm grains) polycrystalline BZY thin film of 6 μm in thickness,[2,25] does show higher activation energy and lower conductivities than the present films (below 700 ºC). However, these values are substantially lower than the conductivities reported for epitaxial films prepared by PLD on MgO (100) by other researchers[10,11], which correlate reasonably well with the extrapolated bulk protonic conductivity of BZY reported by Kreuer[2], which can only be measured at very low temperatures, as shown in Fig. 12.

Bae et al[12] reports very low conductivities of BZY deposited on MgO due to the polycrystalline nature of the films, which is in the same bold part as the nanograined (ca. 30 nm) film by Kreuer. [2] However, these films are different than the epitaxial BZY (100) fabricated in this work. Others report that Ba deficiency plays a critical role in its electrical properties.[26] It is well known that cation non-stoichiometry in Y-doped $BaZrO_3$ leads to a large decrease in conductivity, both for Ba excess and Ba loss in thin films[27] and bulk.[21] The highly conducting BZY thin films are reported in refs.[10,11] Shim et al.[10] showed conductivities in the order of 3 mS/cm at 250 ºC for 60 nm thick BZY films. They report a decrease in ionic conductivity with increasing thickness, although their decrease is not as large as that encountered in this work. On the other hand, Pergolesi et al.[11] showed the highest ever reported conductivities for 1 μm thick BZY films deposited on MgO (100) by PLD, in the order of 100 mS/cm at 500 ºC. As a matter of fact, this highly conducting BZY film[11] used a BZY (20 at.% Y) with a higher dopant concentration than our targets (10 at.% Y). We may also mention that the tetragonal distortion of the BZY films measured in this work is larger than that reported by Pergolesi et al.[11], who also report a larger in-plane (4.21 Å) and larger out-of-plane (4.23 Å) lattice parameters. This may be an indication of changes in the stoichiometry of the films that have yet to be understood.

Investigations of epitaxial thin films cannot exclude effects of strain in the functional properties of the films, which we attempt to mention in the following. The influence of strain on the proton diffusion in BZY has been evaluated by molecular dynamics. Fronzi et al[28] predicted enhanced ionic conductivity caused by a preferential path for proton diffusion under compressive strain conditions. Ottochian et al[29] reported that

moderate compressive isotropic pressure indeed showed to favour proton diffusion by diminishing the oxygen-oxygen distance without affecting the symmetry. They also report that the expected enhancement in proton diffusion under optimized conditions (moderate compressive strain) is only by a factor of two, while higher biaxial compressive and tensile strain lead to a decrease in proton diffusion by inducing a symmetry breaking that results in a strong localization of protons away from the B cations. However, the electrical conductivity of the films in our work is believed to vary more distinctly with the composition and the microstructure of the films and discussing results that solely reflects effects of the strain are not possible with the present set of data. Moreover, a factor of two of maximum possible enhancement of the conductivity is probably difficult to prove experimentally. All in all, this work shows the potential of boosting the functional properties of BZY thin films by a multi-factor optimization of the grown films. We may suggest that further optimization may be achieved by preparing Ba-rich targets of suitable over-stoichiometry and higher Y content, in order to deposit BZY films at higher oxygen partial pressure, which render optimized surface (and likely bulk) properties and, possibly, enhanced protonic conductivity.

Conclusions

We have investigated the influence of growth parameters of BZY thin films by PLD on a number of single crystal substrates and target materials to the functional properties of the films. BZY grows epitaxially on MgO (100), GSO (110), STO (100), NGO (110), and LAO (100), but not on sapphire $(1\bar{1}02)$. The deposition conditions were studied in detail to reveal the influence the morphology, cell parameters and chemical composition on the films´ functional properties. We concluded that the oxygen partial pressure during film growth is the most determining. The BZY thin film protonic conductivity was optimised for films grown at 50 mtorr of O_2, for both the Ni-free and 1% Ni-containing targets, reaching conductivity values and activation energies typical for bulk BZY, although they are lower than those reported by the highest conducting BZY thin films prepared in a similar manner. It is important to highlight that high temperature XRD shows that the expansion of epitaxial films behave different than bulk. BZY films deposited on MgO are special due to the fact that the film is under tensile strain at

high temperature (during operation conditions) while it reverses into compressive strain below 300 °C.

Acknowledgements

AM wishes to thank support from a grant from Iceland, Liechtenstein and Norway through the EEA Financial Mechanism operated by Universidad Complutense de Madrid. This work was further supported by MINECO (project MAT2011-29081-C02-01). ICN2 acknowledges support from the Severo Ochoa Program (MINECO, Grant SEV-2013-0295). Dr. Sandrine Ricote, Dr. Tony Manerbino and Dr. Grover Coors are gratefully acknowledged to provide target bulk samples, Francisco Belarre from ICN2 for careful preparation of samples for TEM observation, and Xavier Llovet from CCiTUB for EPMA measurements.

References

1 E. Fabbri, A. Magrasó, D. Pergolesi, Low-temperature solid-oxide fuel cells based on proton-conducting electrolytes, *MRS Bulletin,* 2014, **39**, 792-797A.

2 K. D. Kreuer, Proton-conducting oxides, *Annu. Rev. Res.*, 2003, **33**, 333-59.

3 P. Babilo, T. Uda, S. M. Haile, Processing of yttrium-doped barium zirconate for high proton conductivity, *J. Mater. Res*., 2007, **22**, 1322-30.

4 S. B. C. Duval, P. Holtappels, U. F. Vogt, E. Pomjakushina, K. Conder, U. Stimming, Electrical conductivity of the proton conductor $BaZr_{0.9}Y_{0.1}O_{3-d}$ obtained by high temperature annealing, *Solid State Ionics*, 2007, **178**, 1437-1441.

5 C. Kjølseth, H. Fjeld, Ø. Prytz, P.I. Dahl, C. Estournès, R. Haugsrud, T. Norby, Space–charge theory applied to the grain boundary impedance of proton conducting $BaZr_{0.9}Y_{0.1}O_{3-\delta}$, *Solid State Ionics*, 2010, **181**, 268-275.

6 I. Kosacki, C. M. Rouleau, P. F. Becher, J. Bentley, D. H. Lowndes, Nanoscale effects on the ionic conductivity in highly textured YSZ thin films, *Solid State Ionics*, 2005, **176**, 1319-1326.

7 J. Garcia-Barriocanal, A. Rivera-Calzada, M. Varela, Z. Sefrioui, E. Iborra, C. Leon, J. Santamaria, Colossal ionic conductivity at interfaces of epitaxial ZrO_2:Y_2O_3/$SrTiO_3$ heterostructures, *Science*, 2008, **321**, 676-680.

8 J. Maier, Ionic conduction in space charge regions, *Prog. Solid St. Chem.*, 1995, **23**, 171-263.

9 N. Schichtel, C. Korte, D. Hesse, and J. Janek. Elastic strain at interfaces and its influence on ionic conductivity in nanoscaled solid electrolyte thin films—theoretical considerations and experimental studies, *Phys. Chem. Chem. Phys.*, 2009, **11**, 3043-3048.

10 J. H. Shim, J. Hyung, T. M. Gür, F. B. Prinz. Proton conduction in thin film yttrium-doped barium zirconate. *Appl. Phys. Lett*. 2008, **92**, 253115.

11 D. Pergolesi, E. Fabbri, A. D'Epifanio, E. Di Bartolomeo, A. Tebano, S. Sanna, E. Traversa, High proton conduction in grain-boundary-free yttrium-doped barium zirconate films grown by pulsed laser deposition, *Nat. Mater*., 2010, **9**, 846–852.

12 K. Bae, D. Y. Jang, S. M. Choi, B. K. Kim, J. H. Lee, J. W. Son, and J. H. Shim, Influence of background oxygen pressure on film properties of pulsed laser deposited Y:$BaZrO_3$, *Thin Solid Films*, 2014, **552**, 24-31.

13 S. Ricote, N. Bonanos, G. Caboche. Water vapour solubility and conductivity study of the proton conductor $BaCe_{(0.9-x)}Zr_xY_{0.1}O_{(3-\delta)}$, *Solid State Ionics*, 2009, **180**, 990-997.

14 S. Ricote, N. Bonanos, A. Manerbino, W. G. Coors. Conductivity study of dense $BaCe_xZr_{(0.9-x)}Y_{0.1}O_{(3-\delta)}$ prepared by solid state reactive sintering at 1500 °C. *International Journal of Hydrogen Energy*, 2012, **37**, 7954-7961.

15 Y. S. Touloukian, R. K. Kirby, R. E. Taylor, T. Y. R. Lee. Thermal expansion-nonmetallic solids. *Thermophysical Properties of Matter*, 1977. 13IFI/Plenum, New York, USA, p 288.

16 A. K. E. Andersson, S. M. Selbach, C. S. Knee, T. Grande. Chemical Expansion Due to Hydration of Proton-Conducting Perovskite Oxide Ceramics. *J. Am. Ceram. Soc*., 2014, **97**, 2654-2661.

17 NIST X-ray Photoelectron Spectroscopy Database. http://srdata.nist.gov/xps/

18 V. P. Gorelov, V. B. Balakireva. Synthesis and Properties of High-Density Protonic Solid Electrolyte $BaZr_{0.9}Y_{0.1}O_{3-d}$. *Rus. J. Electrochem*., 2009, **45**, 476–482.

19 Y. Yamazaki, R. Hernandez-Sanchez, S. M. Haile. High total proton conductivity in large-grained yttrium-doped barium zirconate, *Chem. Mater*. 2009, **21**, 2755-2762.

20 D. Han, K. Kishida, K. Shinoda, H. Inui, T. Uda. A comprehensive understanding of structure and site occupancy of Y in Y-doped $BaZrO_3$, *J. Mater. Chem. A*, 2013, **1**, 3027-3033.

21 Y. Yamazaki, R. Hernandez-Sanchez, S. M. Haile, Cation non-stoichiometry in yttrium-doped barium zirconate: phase behavior, microstructure, and proton conductivity. *J. Mater. Chem.,* 2010, **20**, 8158-8166.

22 E. Kim, Y. Yamazaki, S. M. Haile, H. I. Yoo, Effect of NiO sintering-aid on hydration kinetics and defect-chemical parameters of $BaZr_{0.8}Y_{0.2}O_{3-\Delta}$, *Solid State Ionics*, 2015, **275**, 23-28.

23 J. M. Polfus, K. Toyoura, F. Oba, I. Tanaka, R. Haugsrud, Defect chemistry of a $BaZrO_3$ Σ3 (111) grain boundary by first principles calculations and space–charge theory. *Phys. Chem. Chem. Phys*. 2012, **14**, 12339-12346.

24 K. Katahira, Y. Kohchi, T. Shimura, H. Iwahara. Protonic conduction in Zr-substituted $BaCeO_3$, *Solid State Ionics*, 2000, **138**, 91–98.

25 K. D. Kreuer, personal communication (12/11/2015)

26 H. Bae, Y. Lee, K. J. Kim, G. M. Choi, Effects of Fabrication Conditions on the Crystallinity, Barium Deficiency, and Conductivity of $BaZr_{0.8}Y_{0.2}O_{3-\delta}$ Films Grown by Pulsed Laser Deposition, *Fuel Cells*, 2015, **15**, 408-415.

27 J. S. Park, Y. B. Kim, J. An, J. H. Shim, T. M. Gür, F. B. Prinz, Effect of cation non-stoichiometry and crystallinity on the ionic conductivity of atomic layer deposited Y: $BaZrO_3$ films, *Thin Solid Films*, 2013, **539**, 166-169.

28 M. Fronzi, Y. Tateyama, N. Marzari, E. Traversa. First-principles molecular dynamics simulations of proton diffusion in cubic $BaZrO_3$ perovskite under strain conditions. *arXiv*:1309.5200, 2013.